Nonlinear wind-induced instability of orthotropic plane membrane structures

Changjiang Liu[1,2], Feng Ji[*1], Zhoulian Zheng[3], Yuyou Wu[4] and Jianjun Guo[5]

[1]*State Key Laboratory of Geohazard Prevention and Geoenvironment Protection,*
Chengdu University of Technology, Chengdu, 610059, China
[2]*Department of Structural Engineering, University of California, San Diego, La Jolla, CA 92093, USA*
[3]*College of Civil Engineering, Chongqing University, Chongqing, 400045, China*
[4]*Department of Buildings, Shenzhen Institute of Urban Safety, Shenzhen, Guangdong, 518000, China*
[5]*Chongqing Water Resources and Electric Engineering College, Yongchuan, Chongqing, 402160, China*

Abstract.   The nonlinear aerodynamic instability of a tensioned plane orthotropic membrane structure is theoretically investigated in this paper. The interaction governing equation of wind-structure coupling is established by the Von Kármán's large amplitude theory and the D'Alembert's principle. The aerodynamic force is determined by the potential flow theory of fluid mechanics and the thin airfoil theory of aerodynamics. Then the interaction governing equation is transformed into a second order nonlinear differential equation with constant coefficients by the Bubnov-Galerkin method. The critical wind velocity is obtained by judging the stability of the second order nonlinear differential equation. From the analysis of examples, we can conclude that it's of great significance to consider the orthotropy and geometrical nonlinearity to prevent the aerodynamic instability of plane membrane structures; we should comprehensively consider the effects of various factors on the design of plane membrane structures; and the formula of critical wind velocity obtained in this paper provides a more accurate theoretical solution for the aerodynamic stability of the plane membrane structures than the previous studies.

Keywords: membrane structures; orthotropy; nonlinearity; wind-induced instability; critical wind velocity

1. Introduction

The building membrane structure has become popular during the last few decades. Because of its economy, beauty, and light weight, it is widely applied in large span structures, such as stadiums, terminal buildings, exhibition centers and works of art, etc. However membrane structure is very sensitive to the wind load because of its light weight, low stiffness and low natural frequency. Therefore, the wind load is the main control load of the membrane structure, and the aerodynamic instability may occur when the wind velocity reaches a certain value (Miyake *et al.* 1992, Kawakita *et al.* 1992).

In engineering practices, the main stadium of American Atlanta Olympics (Georgia Dome) was

---

∗Corresponding author, Associate Professor, E-mail: jeifens@163.com

destroyed by strong winds in 1995; the openable membrane roof of Montreal Olympic Stadium in Canada was slitted in a snowstorm in 1999; the membrane roofs of the Cheju World Cup stadium in Korea and Wenzhou University stadium in China were also locally destroyed by the wind loads in 2002 and 2004, respectively. In addition to these incidences, there were many other analogous wind-induced accidents of membrane structures (Luo 2006). It is noteworthy that the wind-resistant designs were carried out for these structures before their construction, but the wind-induced damage still occurred under the condition of the local wind velocity lower than the design critical wind velocity. This phenomenon has attracted the scholars' great attention to explore the aerodynamic instability mechanism of this kind of structures under wind load.

At present, relatively consistent view is that the membrane structure vibrates mainly in single mode for divergence instability under a lower wind velocity, and it presents a trend of multi-mode coupling for flutter instability with the increasing of the wind velocity (Minarni *et al.* 1993, Sun *et al.* 2003). However, due to the complexity of the problem, the studies on the quantitative analysis are poor.

Sygulski (1994, 1997) derived the critical instability wind velocity of a piece of membrane supported on a rigid board in the uniform potential flow by applying the finite element method and boundary element method. Sygulski (1996) investigated the aeroelastic dynamic stability of the vibration of a three-dimensional pneumatic structure in wind flow, and the analytical prediction is in agreement with observation of wind-tunnel experiments. Glück *et al.* (2001) presented a numerical method of a time-dependent fluid-structure coupling for membrane and thin shell structures with large displacements; and this coupled algorithm provides some reference for the calculation of fluid-structure interaction of analogous structures. Attar *et al.* (2005) applied a reduced order system identifying approach to analyze the structural nonlinear behavior of aeroelastic configurations; and the results agreed well with those from a high-fidelity aeroelastic model. Stanford *et al.* (2007, 2008) constructed a novel experimental facility that integrated a wind tunnel with a visual image correlation system for simultaneous measurement of wing displacements, strains, and aerodynamic loads, and the numerical and experimental data have suitable correspondence for moderate angles of attack. Combined with a finite difference membrane model with 3rd order piston theories, Scott *et al.* (2007) applied NASTRAN normal modes in the structured compressible flow solver to simulate the dynamic aeroelastic stability of membrane structures for aero-capture, and the results obtained are well consistent with a static aeroelastic analysis. Michalski *et al.* (2011) outlined a virtual design method by fluid–structure interaction simulation for membrane structures under the impact of fluctuating wind loads and provided results on the unique validation of this method at real-scale tests of a highly flexible 29 m umbrella, and the comparative analysis proved the effectiveness of this method. Lu *et al.* (2013) and Sun *et al.* (2014) studied the fluid-structure interaction (FSI) of membrane structures under wind actions by novel numerical method, and obtained some significant results for the wind-resistant design of membrane structures. Zhou *et al.* (2014) established a framework to numerically analyze the added mass of open flat membranes by using the boundary element method, and the comparison between numerical and experimental results showed the added mass only considering the effect of geometric shape can agree well with the test results in low-order modes. Wu *et al.* (2015) studied the aero-elastic instability characteristics and mechanism of two closed-type saddle-shaped tensioned membrane structures by wind tunnel test, and obtained some significant conclusions.

Additionally, some significant analytical studies were carried out for the aerodynamic instability of membrane structures. Yang and Liu (2005) applied the non-moment theory of thin

shallow shells and the potential flow theory in fluids to study the aerodynamic instability critical wind velocity of three-dimensional membrane structures, and the linear instability critical wind velocity is obtained by Routh-Hurwitz stability criterion. Wu *et al*. (2008) presented a computational method for simulating the wind-structure interaction effects of tension structures, and the results provide some significance basis for the computation of wind-introduced instability critical wind velocity. Zheng *et al*. (2011) adopted the similar analytical approach to obtain the nonlinear critical wind velocity of planar orthotropic membrane structures in large amplitude theory; and then their further research obtained the analytical solution of the nonlinear critical wind velocity of the hyperbolic paraboloid orthotropic membrane structure (Xu *et al*. 2011). However the stress function in their study did not fully satisfy the stress boundary conditions, so their results are not complete and need further amendment.

   In this paper we theoretically study the aerodynamic stability of the tensioned plane membrane structure and propose a new stress function that fully satisfies the stress boundary conditions for further study. The governing equation is derived by the von Kármán's large amplitude theory and D'Alembert's principle. The critical instability wind velocity is obtained by judging the stability of the governing equation. Through the parametric analysis, some significant conclusions are obtained for the wind-resistant design of the plane membrane structure. The analytical method herein provides favorable reference for the stability analysis of the analogous structures.

2. Structural model and governing equations

   The studied structure model is a rectangular plane membrane structure with its four edges simply supported as shown in Fig. 1. The membrane material is orthotropic and its two orthogonal directions are x and y directions with different Young's modulus. a and b denote the spans in x and y directions, respectively. N_{0x} and N_{0y} denote the initial stress in x and y directions, respectively. Point O is the original point of xoy coordinate system. The wind direction is x direction and its velocity is V.

   According to the von Kármán's large amplitude theory and D'Alembert's principle (Liu *et al*. 2013, 2014), the dynamic motion equation and compatible equation of the orthotropic membrane are

$$\begin{cases} \rho_0 \dfrac{\partial^2 w}{\partial t^2} + 2\rho_0 \xi_0 \dfrac{\partial w}{\partial t} - \left(N_x + N_{0x}\right)\dfrac{\partial^2 w}{\partial x^2} - \left(N_y + N_{0y}\right)\dfrac{\partial^2 w}{\partial y^2} + 2N_{xy}\dfrac{\partial^2 w}{\partial x \partial y} = p_z(t) \\[4mm] \dfrac{1}{E_1 h}\dfrac{\partial^2 N_x}{\partial y^2} + \dfrac{1}{E_2 h}\dfrac{\partial^2 N_y}{\partial x^2} - \dfrac{\mu_1}{E_1 h}\dfrac{\partial^2 N_x}{\partial x^2} - \dfrac{\mu_2}{E_2 h}\dfrac{\partial^2 N_y}{\partial y^2} - \dfrac{1}{Gh}\dfrac{\partial^2 N_{xy}}{\partial x \partial y} = \left(\dfrac{\partial^2 w}{\partial x \partial y}\right)^2 - \dfrac{\partial^2 w}{\partial x^2}\dfrac{\partial^2 w}{\partial y^2} \end{cases} \tag{1}$$

where ρ_0 is the areal density of membrane; w is the deflection: $w(x, y, t)$; ξ_0 is the damping coefficient of the structure; N_x and N_y are the stress increments in x and y directions, respectively; N_{xy} is the shear stress; N_{0x} and N_{0y} are the initial stress in x and y directions, respectively; h is the membrane's thickness; E_1 and E_2 are the Young's modulus in x and y direction, respectively; G is the shear modulus; μ_1 and μ_2 are the Poisson's ratio in x and y directions, respectively; $p_z(t)$ is the external load in z direction.
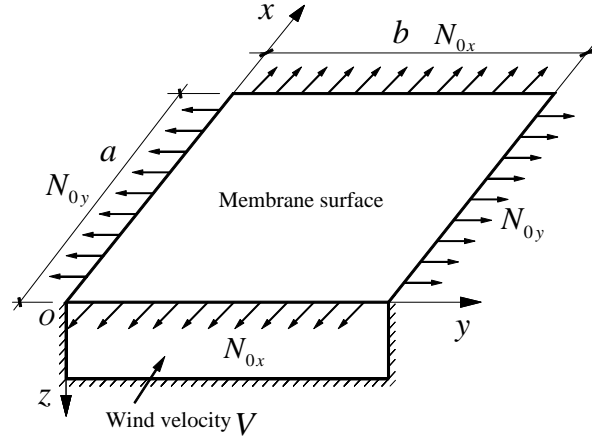
Fig. 1 Tensioned orthotropic plane membrane model with four edges clamped

The introduction of stress function $\varphi = \varphi(x, y, t)$ yields

$$
\begin{cases}
N_x = h \dfrac{\partial^2 \varphi}{\partial y^2} \\[2mm]
N_y = h \dfrac{\partial^2 \varphi}{\partial x^2} \\[2mm]
N_{xy} = -h \dfrac{\partial^2 \varphi}{\partial x \partial y}
\end{cases}
\tag{2}
$$

The maximum vibration displacement of the membrane is much smaller than the boundary size, so the shearing actions among the membrane fibers are very small, and the effect of shearing stresses is thus assumed negligible, i.e., $N_{xy} = 0$ (Zheng *et al.* 2011, Xu *et al.* 2011). Therefore

$$
\frac{\partial^2 N_x}{\partial x^2} = \frac{\partial^2 N_y}{\partial y^2} = h \frac{\partial^4 \varphi}{\partial x^2 \partial y^2} = -\frac{\partial^2 N_{xy}}{\partial x \partial y} = 0
\tag{3}
$$

The external load $p_z(t)$ can be expressed as follows

$$
p_z(t) = p_2 - p_1
\tag{4}
$$

where p_1 and p_2 are the pressure on the lower and upper surface, respectively; and p_1 approximately equals the static atmospheric pressure p_∞.

By substituting Eqs. (2)-(4) into Eq. (1), one obtains

$$
\left(h \frac{\partial^2 \varphi}{\partial y^2} + N_{0x} \right) \frac{\partial^2 w}{\partial x^2} + \left(h \frac{\partial^2 \varphi}{\partial x^2} + N_{0y} \right) \frac{\partial^2 w}{\partial y^2} - 2\rho_0 \xi_0 \frac{\partial w}{\partial t} + p_2 - p_1 = \rho_0 \frac{\partial^2 w}{\partial t^2}
\tag{5}
$$

$$\frac{1}{E_1}\frac{\partial^4 \varphi}{\partial y^4} + \frac{1}{E_2}\frac{\partial^4 \varphi}{\partial x^4} = \left(\frac{\partial^2 w}{\partial x \partial y}\right)^2 - \frac{\partial^2 w}{\partial x^2}\frac{\partial^2 w}{\partial y^2} \tag{6}$$

The membrane structure is a typical flexible structure, and its bending resistance is so weak that the bending resistance of the membrane is neglected in this paper. Therefore, the boundary of the studied membrane structural model is considered as simply supported. Thus the displacement and bending moment are equal to zero, i.e. the boundary condition (7). In Eq. (7), the second order derivatives of w are equal to zero, which means the bending moments on the boundary is zero. Even if there are initial stress N_{0x} and N_{0y} in the membrane, the stress increment N_x and N_y on the boundary are zero, which is expressed by the boundary condition (8).

The corresponding displacement and stress boundary conditions can be expressed as:

$$\begin{cases} w(0,y,t)=0, & \dfrac{\partial^2 w}{\partial x^2}(0,y,t)=0 \\ w(a,y,t)=0, & \dfrac{\partial^2 w}{\partial x^2}(a,y,t)=0 \end{cases}, \quad \begin{cases} w(x,0,t)=0, & \dfrac{\partial^2 w}{\partial y^2}(x,0,t)=0 \\ w(x,b,t)=0, & \dfrac{\partial^2 w}{\partial y^2}(x,b,t)=0 \end{cases} \tag{7}$$

$$\begin{cases} \dfrac{\partial^2 \varphi}{\partial x^2}(0,y,t)=0 \\ \dfrac{\partial^2 \varphi}{\partial x^2}(a,y,t)=0 \end{cases}, \quad \begin{cases} \dfrac{\partial^2 \varphi}{\partial y^2}(x,0,t)=0 \\ \dfrac{\partial^2 \varphi}{\partial y^2}(x,b,t)=0 \end{cases} \tag{8}$$

3. Determination of aerodynamic force

The air viscosity should be considered if the vibration wavelength is close to the air boundary layer thickness (Dowell *et al*. 1970). But the low-order modes often play a dominant role in the vibration of civil engineering structures, so the vibration wavelength is far larger than the boundary layer thickness. Meanwhile, the experimental studies of Uematsu *et al*. (1986) showed that the turbulence in the boundary layer has slight effect on the wind-induced structural response. Therefore, the potential flow can be considered as inviscid, stationary, uniform and incompressible in this paper. Assume that the flow acts on the upper surface of the structure only, and the direction of the flow velocity V is x-axis direction (as shown in Fig.1).

According to the fluid Bernoulli Equation, the outdoor (upper surface) pressure p_2 is (Forsching 1982)

$$p_2 = -\rho\left(V\frac{\partial \phi'}{\partial x} + \frac{\partial \phi'}{\partial t}\right)_{z=z_0} + p_\infty \tag{9}$$

where ρ is the air density; $\phi' = \phi'(x,y,z,t)$ is the perturbed velocity potential function;

$z_0 = z_0(x, y)$ is the surface function under initial stress; p_∞ is the static atmospheric pressure.

According to the potential theory, $\phi'(x, y, z, t)$ in Eq. (9) must satisfy the Laplace's equation (10) and boundary condition (11).

$$\frac{\partial^2 \phi'}{\partial x^2} + \frac{\partial^2 \phi'}{\partial y^2} + \frac{\partial^2 \phi'}{\partial z^2} = 0 \tag{10}$$

$$v_z = \frac{\partial \phi'}{\partial z} = 2\left(V \frac{\partial z}{\partial x} + \frac{\partial z}{\partial t} \right) \tag{11}$$

where v_z is the flow velocity component in z direction.

According to the thin airfoil theory of aerodynamics, $\phi'(x, y, z, t)$ that satisfies Eqs. (10) and (11) can be expressed as follows (Ivovich *et al.* 1991)

$$\phi'(x, y, z, t) = \frac{1}{2\pi} \iint_{Ra} \frac{\left(V \frac{\partial z}{\partial x} + \frac{\partial z}{\partial t} \right)_{\substack{x=\xi \\ y=\eta}}}{\sqrt{(x-\xi)^2 + (y-\eta)^2}} d\xi d\eta \tag{12}$$

where Ra denotes the structural projection area in the plane xoy.

The membrane surface function under wind loadings is

$$z(x, y, t) = z_0(x, y) + w(x, y, t) \tag{13}$$

Because the studied membrane is plane, $z_0(x, y) = 0$. Then we obtain

$$z(x, y, t) = w(x, y, t) \tag{14}$$

By substituting Eq. (14) into (12), one obtains

$$p_2 = -\frac{\rho}{2\pi} \left(-V \iint_{Ra} \frac{\left(V \frac{\partial w}{\partial x} + \frac{\partial w}{\partial t} \right)_{\substack{x=\xi \\ y=\eta}} (x-\xi)}{\left(\sqrt{(x-\xi)^2 + (y-\eta)^2} \right)^3} d\xi d\eta + \iint_{Ra} \frac{\left(V \frac{\partial^2 w}{\partial x \partial t} + \frac{\partial^2 w}{\partial t^2} \right)_{\substack{x=\xi \\ y=\eta}}}{\sqrt{(x-\xi)^2 + (y-\eta)^2}} d\xi d\eta \right) + p_\infty \tag{15}$$

Let

$$A_1 = \frac{\rho + \rho^*}{2\pi} \iint_{Ra} \frac{1}{r} \left(\frac{\partial^2 w}{\partial t^2} \right)_{\substack{x=\xi \\ y=\eta}} d\xi d\eta, \qquad A_2 = \frac{\rho V}{2\pi} \iint_{Ra} \frac{1}{r} \left(\frac{\partial^2 w}{\partial x \partial t} \right)_{\substack{x=\xi \\ y=\eta}} d\xi d\eta$$

$$A_3 = \frac{\rho V^2}{2\pi} \iint_{Ra} \frac{1}{r^3} \left(\frac{\partial w}{\partial x} \right)_{\substack{x=\xi \\ y=\eta}} (x-\xi) d\xi d\eta, \qquad A_4 = \frac{\rho V}{2\pi} \iint_{Ra} \frac{1}{r^3} \left(\frac{\partial w}{\partial t} \right)_{\substack{x=\xi \\ y=\eta}} (x-\xi) d\xi d\eta$$

$$r = \sqrt{(x-\xi)^2 + (y-\eta)^2}$$

where $Ra \in \{0 \leq \xi \leq a, 0 \leq \eta \leq b\}$, the gas inertial load ρ^* which attached to the lower surface is taken into consideration in A_1 (Yang and Liu 2005), and assume $\rho^* = \rho$.

Then Eq. (15) can be simplified as

$$p_2 = -A_1 - A_2 + A_3 + A_4 + p_\infty \tag{16}$$

The substitution of Eq. (16) into Eq. (5) yields

$$\left(h\frac{\partial^2 \varphi}{\partial y^2} + N_{0x} \right)\frac{\partial^2 w}{\partial x^2} + \left(h\frac{\partial^2 \varphi}{\partial x^2} + N_{0y} \right)\frac{\partial^2 w}{\partial y^2} - 2\rho_0 \xi_0 \frac{\partial w}{\partial t}$$
$$= \rho_0 \frac{\partial^2 w}{\partial t^2} + A_1 + A_2 - A_3 - A_4 \tag{17}$$

4. Critical wind velocity of instability

The functions that satisfy the boundary conditions Eq. (7) are separated as follows (Liu *et al.* 2013, 2014)

$$w(x, y, t) = \sum_{m,n} T_{mn}(t) \cdot W_{mn}(x, y) \tag{18}$$

where $W_{mn}(x, y)$ is the given mode shape function; $T_{mn}(t)$ is function of time; m and n are positive integer.

According to the basic vibration theory, the mode shape function is given by

$$W(x, y) = \sin\frac{m\pi x}{a} \sin\frac{n\pi y}{b} \tag{19}$$

where m and n denote the orders of vibration mode in x and y directions, respectively. Eq. (19) satisfies the boundary conditions automatically.

We take one term of Eq. (18) for computation, i.e.

$$w(x, y, t) = T_{mn}(t)\sin\frac{m\pi x}{a} \sin\frac{n\pi y}{b} \tag{20}$$

In order to simplify the computation symbols, we let $W_{mn}(x, y) = W(x, y) = W$, $T_{mn}(t) = T(t) = T$.

The substitution of Eq. (20) into Eq. (6) yields

$$\frac{1}{E_1}\frac{\partial^4 \varphi}{\partial y^4} + \frac{1}{E_2}\frac{\partial^4 \varphi}{\partial x^4} = \frac{m^2 n^2 \pi^4}{2a^2 b^2} T^2(t)\left(\cos\frac{2m\pi x}{a} + \cos\frac{2n\pi y}{b} \right) \tag{21}$$

The studied model is a symmetrical structure, so the stress function φ should be an even

function and satisfy the stress boundary condition (7). Therefore, the stress function can be assumed as follows

$$\varphi(x,y,t) = T^2(t)\left(\alpha \cos\frac{2m\pi x}{a} + \beta \cos\frac{2n\pi y}{b} + \chi_1 x^2 + \chi_2 y^2 \right) \tag{22}$$

The substitution of Eq. (22) into Eqs. (21) and (7) yields

$$\alpha = \frac{E_2 n^2 a^2}{32 m^2 b^2}, \quad \beta = \frac{E_1 m^2 b^2}{32 n^2 a^2}, \quad \chi_1 = \frac{\pi^2 E_2 n^2}{16 b^2}, \quad \chi_2 = \frac{\pi^2 E_1 m^2}{16 a^2}$$

Then the stress function is

$$\varphi(x,y,t) = \left(\frac{E_2 n^2 a^2}{32 m^2 b^2} \cos\frac{2m\pi x}{a} + \frac{E_1 m^2 b^2}{32 n^2 a^2} \cos\frac{2n\pi y}{b} + \frac{\pi^2 E_2 n^2 x^2}{16 b^2} + \frac{\pi^2 E_1 m^2 y^2}{16 a^2} \right) T^2(t) \tag{23}$$

The substitution of Eqs. (20) and Eq. (23) into Eq. (17) yields

$$\left(\rho_0 W + \frac{\rho}{\pi}\gamma_1 \right) T''(t) + \left[\frac{\rho V}{2\pi}(\gamma_2 - \gamma_4) + 2\rho_0 \xi_0 W \right] T'(t)$$

$$- \left(N_{0x}\frac{\partial^2 W}{\partial x^2} + N_{0y}\frac{\partial^2 W}{\partial y^2} + \frac{\rho V^2}{2\pi}\gamma_3 \right) T(t) - h\left(\frac{\partial^2 \Phi}{\partial y^2}\frac{\partial^2 W}{\partial x^2} + \frac{\partial^2 \Phi}{\partial x^2}\frac{\partial^2 W}{\partial y^2} \right) T^3(t) = 0 \tag{24}$$

where

$$T''(t) = \frac{d^2 T(t)}{dt^2}, \quad T'(t) = \frac{dT(t)}{dt}$$

$$\gamma_1 = \iint\limits_{Ra} \frac{1}{r}(W)_{\substack{x=\xi \\ y=\eta}} d\xi d\eta = \iint\limits_{Ra} \frac{1}{r}\sin\frac{m\pi\xi}{a}\sin\frac{n\pi\eta}{b} d\xi d\eta$$

$$\gamma_2 = \iint\limits_{Ra} \frac{1}{r}\left(\frac{\partial W}{\partial x} \right)_{\substack{x=\xi \\ y=\eta}} d\xi d\eta = \frac{m\pi}{a}\iint\limits_{Ra} \frac{1}{r}\cos\frac{m\pi\xi}{a}\sin\frac{n\pi\eta}{b} d\xi d\eta$$

$$\gamma_3 = \iint\limits_{Ra} \frac{1}{r^3}\left(\frac{\partial W}{\partial x} \right)_{\substack{x=\xi \\ y=\eta}} (x-\xi) d\xi d\eta$$

$$= \frac{m\pi}{a}\iint\limits_{Ra} \frac{1}{r^3}(x-\xi)\cos\frac{m\pi\xi}{a}\sin\frac{n\pi\eta}{b} d\xi d\eta$$

$$\gamma_4 = \iint\limits_{Ra} \frac{1}{r^3}(W)_{\substack{x=\xi \\ y=\eta}} (x-\xi) d\xi d\eta$$

$$= \iint\limits_{Ra} \frac{1}{r^3}(x-\xi)\sin\frac{m\pi\xi}{a}\sin\frac{n\pi\eta}{b} d\xi d\eta$$

According to the Bubnov-Galerkin method (Shin *et al*. 2004), Eq. (24) can be transformed as follows

$$\iint\limits_{S}\left\{\begin{array}{l}\left[\left(\rho_0 W+\dfrac{\rho}{\pi}\gamma_1\right)T''(t)+\left[\dfrac{\rho V}{2\pi}(\gamma_2-\gamma_4)+2\rho_0\xi_0 W\right]T'(t)\right.\\[2mm]\left.-\left(N_{0x}\dfrac{\partial^2 W}{\partial x^2}+N_{0y}\dfrac{\partial^2 W}{\partial y^2}+\dfrac{\rho V^2}{2\pi}\gamma_3\right)T(t)-h\left(\dfrac{\partial^2\Phi}{\partial y^2}\dfrac{\partial^2 W}{\partial x^2}+\dfrac{\partial^2\Phi}{\partial x^2}\dfrac{\partial^2 W}{\partial y^2}\right)T^3(t)=0\end{array}\right\}W(x,y)dxdy=0 \tag{25}$$

where $S\in\{0\le x\le a, 0\le y\le b\}$.

Eq. (25) can be simplified as follows

$$AT''(t)+BT'(t)-CT(t)-DT^3(t)=0 \tag{26}$$

where

$$A=\iint\limits_{S}\left(\rho_0 W+\frac{\rho}{\pi}\gamma_1\right)W dxdy$$

$$=\rho_0\iint\limits_{S}\left(\sin\frac{m\pi x}{a}\sin\frac{n\pi y}{b}\right)^2 dxdy+$$

$$\frac{\rho}{\pi}\iint\limits_{S}\left(\iint\limits_{Ra}\frac{1}{r}\sin\frac{m\pi\xi}{a}\sin\frac{n\pi\eta}{b}d\xi d\eta\right)\sin\frac{m\pi x}{a}\sin\frac{n\pi y}{b}dxdy=\frac{\rho_0 ab}{4}+\frac{\rho}{\pi}\alpha_1$$

$$\alpha_1=\iint\limits_{S}\left(\iint\limits_{Ra}\frac{1}{r}\sin\frac{m\pi\xi}{a}\sin\frac{n\pi\eta}{b}d\xi d\eta\right)\sin\frac{m\pi x}{a}\sin\frac{n\pi y}{b}dxdy$$

$$B=\frac{\rho V}{2\pi}\iint\limits_{S}(\gamma_2-\gamma_4)W dxdy+2\rho_0\xi_0\iint\limits_{S}W^2 dxdy$$

$$=\frac{\rho m V}{2a}\iint\limits_{S}\left(\iint\limits_{Ra}\frac{1}{r}\cos\frac{m\pi\xi}{a}\sin\frac{n\pi\eta}{b}d\xi d\eta\right)\sin\frac{m\pi x}{a}\sin\frac{n\pi y}{b}dxdy$$

$$-\frac{\rho V}{2\pi}\iint\limits_{S}\left\{\iint\limits_{Ra}\frac{1}{r^3}(x-\xi)\sin\frac{m\pi\xi}{a}\sin\frac{n\pi\eta}{b}d\xi d\eta\right\}\sin\frac{m\pi x}{a}\sin\frac{n\pi y}{b}dxdy$$

$$+2\rho_0\xi_0\iint\limits_{S}\left(\sin\frac{m\pi x}{a}\sin\frac{n\pi y}{b}\right)^2 dxdy=\frac{\rho m V}{2a}\alpha_2-\frac{\rho V}{2\pi}\alpha_4+\frac{\rho_0\xi_0 ab}{2}$$

$$\alpha_2=\iint\limits_{S}\left(\iint\limits_{Ra}\frac{1}{r}\cos\frac{m\pi\xi}{a}\sin\frac{n\pi\eta}{b}d\xi d\eta\right)\sin\frac{m\pi x}{a}\sin\frac{n\pi y}{b}dxdy$$

$$\alpha_4=\iint\limits_{S}\left\{\iint\limits_{Ra}\frac{1}{r^3}(x-\xi)\sin\frac{m\pi\xi}{a}\sin\frac{n\pi\eta}{b}d\xi d\eta\right\}\sin\frac{m\pi x}{a}\sin\frac{n\pi y}{b}dxdy$$

$$C = \iint_S \left[\left(hk_{0x}\delta + N_{0y} \right) \frac{\partial^2 W}{\partial y^2} + \left(hk_{0y}\delta + N_{0x} \right) \frac{\partial^2 W}{\partial x^2} + \frac{\rho V^2}{2\pi} \gamma_3 \right] W dx dy$$

$$= \iint_S \left(N_{0x} \frac{\partial^2 W}{\partial x^2} + N_{0y} \frac{\partial^2 W}{\partial y^2} + \frac{\rho V^2}{2\pi} \gamma_3 \right) W dx dy$$

$$= -\frac{m^2 \pi^2 b N_{0x}}{4a} - \frac{n^2 \pi^2 a N_{0y}}{4b} + \frac{\rho m V^2}{2a} \alpha_3$$

$$\alpha_3 = \iint_S \left\{ \iint_{Ra} \frac{1}{r^3} (x-\xi) \cos \frac{m\pi\xi}{a} \sin \frac{n\pi\eta}{b} d\xi d\eta \right\} \sin \frac{m\pi x}{a} \sin \frac{n\pi y}{b} dx dy$$

$$D = h \iint_S \left(\frac{\partial^2 \Phi}{\partial y^2} \frac{\partial^2 W}{\partial x^2} + \frac{\partial^2 \Phi}{\partial x^2} \frac{\partial^2 W}{\partial y^2} \right) W(x,y) dx dy = -\frac{3\pi^4 ab}{64} \left(\frac{E_1 m^4}{a^4} + \frac{E_2 n^4}{b^4} \right)$$

Since that $A > 0$ ($A \leq 0$ may occur only when $b/a \ll 0.1$, but it would not occur in engineering practices), Eq. (26) can be transformed into

$$T''(t) + gT'(t) - cT(t) - dT^3(t) = 0 \tag{27}$$

where $g = \dfrac{B}{A}, c = \dfrac{C}{A}, d = \dfrac{D}{A}$.

Obviously, Eq. (27) is a nonlinear differential equation with respect to $T(t)$, assume that the periodic solution which satisfies the initial condition $T(t)|_{t=0} = 0$ is

$$T(t) = f \cdot \sin \omega t = f \cdot \sin \theta \tag{28}$$

where f denotes the amplitude.

By substituting Eq. (28) into Eq. (27), and applying the Bubnov-Galerkin method again, one obtains

$$\int_0^{T_0} \left[T''(t) + gT'(t) - cT(t) - dT^3(t) \right] \sin\theta dt$$

$$= \int_0^{T_0} \left(-f\omega^2 \sin\theta + g \cdot f\omega\cos\theta - c \cdot f \sin\theta - d \cdot f^3 \sin^3\theta \right) \sin\theta dt$$

$$= -f\int_0^{T_0} (\omega^2 + c + \frac{3}{4} d \cdot f^2) \sin^2\theta dt + g \cdot f\omega\int_0^{T_0} \cos\theta\sin\theta dt + \frac{1}{4} e \cdot f^3 \int_0^{T_0} \sin 3\theta \sin\theta dt$$

$$= -f\int_0^{T_0} (\omega^2 + c + \frac{3}{4} d \cdot f^2) \sin^2\theta dt = 0$$

$$\tag{29}$$

where T_0 is a cycle time, $T_0 = 2\pi/\omega$.

By integrating and simplifying Eq. (29), one obtains

$$\omega^2 = -\left(c + \frac{3}{4} d \cdot f^2 \right) \tag{30}$$

When the wind velocity approaches a certain value (critical value), the aerodynamic force will equal or even exceed the sum of deadweight and inertia force of the structure. This indicates that the divergence instability occurs. Then the frequency of the characteristic equation of the system becomes zero (Kornecki *et al.* 1976). Therefore, the critical condition for divergence instability is $\omega = 0$.

By substituting A, C, D and $\omega = 0$ into Eq. (30), we can obtain the critical wind velocity of divergence instability

$$V_{cr} = \pi \sqrt{\frac{\left(m^2 b N_{0x} + n^2 a^2 N_{0y}/b\right)/2 + 9hm^2 n^2 \pi^2 f^2 (\alpha + \beta)/4b}{\rho m \alpha_3}} \ . \tag{31}$$

If wind velocity $V > V_{cr}$, the divergence instability will occur, whereas if wind velocity $V < V_{cr}$, the structure will be stable and safe.

The critical wind velocity of divergence instability in previous study (Zheng *et al.* 2011) is

$$V_{cr}' = \pi \sqrt{\frac{\left(m^2 b N_{0x} + n^2 a^2 N_{0y}/b\right)/2 + 3hm^2 n^2 \pi^2 f^2 (\alpha + \beta)/4b}{\rho m \alpha_3}} \tag{32}$$

5. Analytical examples and discussion

Take a membrane material which is commonly applied in building structures as an example.
The basic parameters are E_1=1520 MPa, E_2=1290 MPa, h=0.82 mm, ρ=1.226 kg/m³. Let $\lambda = b/a$ (the ratio of cross-wind (*y*) span to along-wind (*x*) span), $\gamma = N_{0x}/N_{0y}$ (the ratio of prestress in *x-direction* to *y-direction*). The value of α_3 is obtained by numerical integration method (Mathematica program) when all the parameters are determined. Then the critical velocities will be calculated by Eqs. (31) and (32) for analyzing the effect of these parameters.
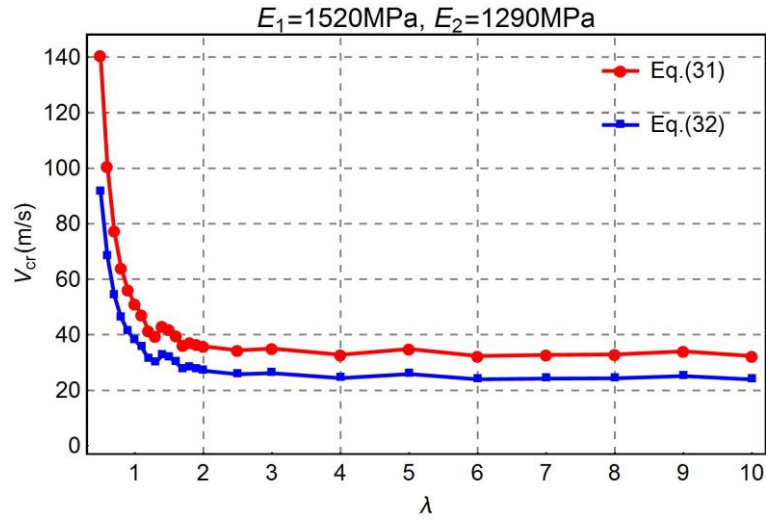
5.1 Span ratio λ

Let a =20 m, m=n=1, γ =1, f =1 m, N_{0x} =2 kN/m. Then the curves of span ratio and critical wind velocity are calculated by Eqs. (31) and (32) and shown in Fig. 2. The span ratio λ increased from 0.5 to 10.

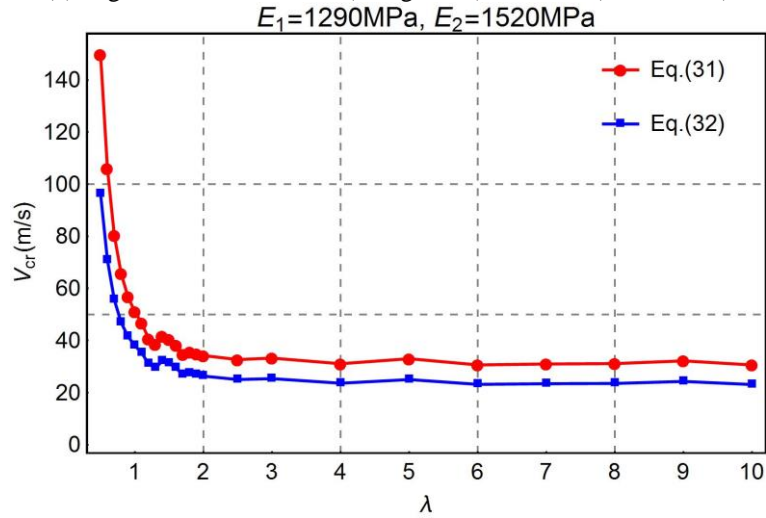From Fig. 2, we can see that the critical wind velocities of the two conditions all decrease gradually. When $\lambda < 1$, the critical wind velocities decrease sharply, and when $\lambda > 1$, the critical wind velocities decrease gently in general. When $\lambda = 1$, the critical wind velocities of Eq. (31) of the two conditions are equal to 51.04 m/s; and the critical wind velocities of Eq. (32) of the two conditions are equal and equal to 38.04 m/s.

From Fig. 2, we can also conclude that: when $\lambda < 1$, a greater critical wind velocity V_{cr} can be obtained if the smaller modulus is arranged in the along-wind direction ($E_1 < E_2$), and the

smaller λ is, the greater V_{cr} is. The situation is just right opposite when $\lambda > 1$, namely, a greater critical wind velocity V_{cr} can be obtained if the greater modulus is arranged in the along-wind direction ($E_1 > E_2$). In addition, the critical wind velocity values that calculated by Eq. (31) are all greater than the corresponding results that calculated by Eq. (32), and the relative differences between them decreases with increasing of the span ratio λ. When λ=0.5, the relative differences are 34.84% (condition 1) and 35.67% (condition 2); and when λ=10, the relative differences are 26.14% (condition 1) and 24.50% (condition 2).

(a) Higher modulus in the x (along-wind) direction (condition 1)

(b) Lower modulus in the x (along-wind) direction (condition 2)

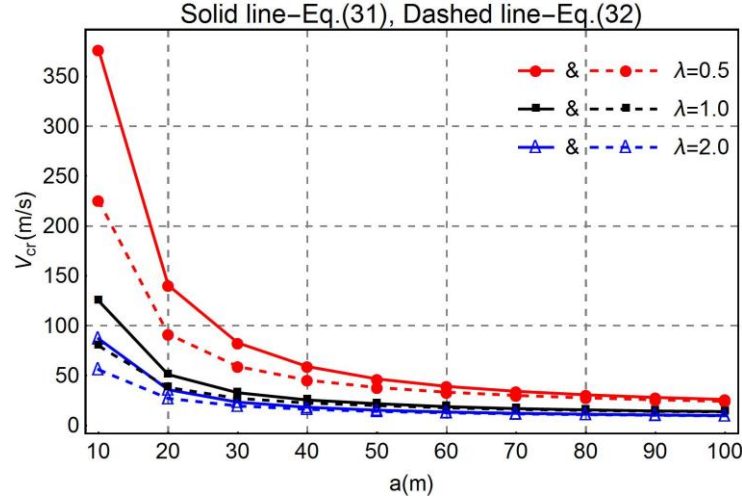Fig. 2. Curves of span ratio λ and critical wind velocity V_{cr}

Fig. 3 Curves of along-wind span a and critical wind velocity V_{cr}
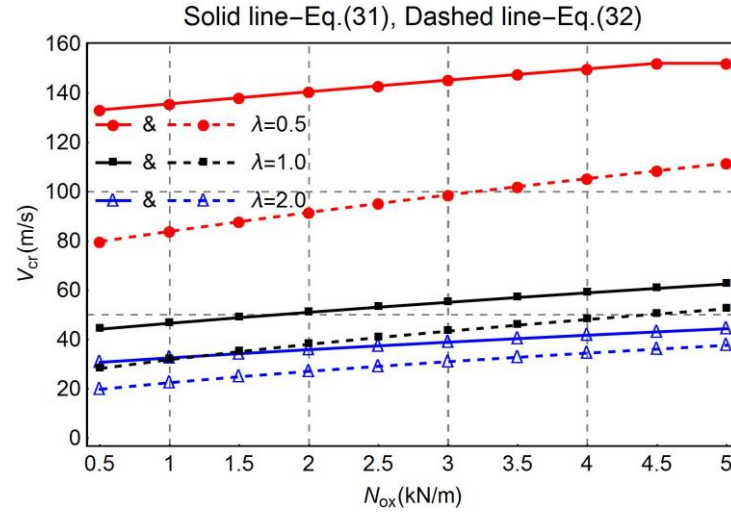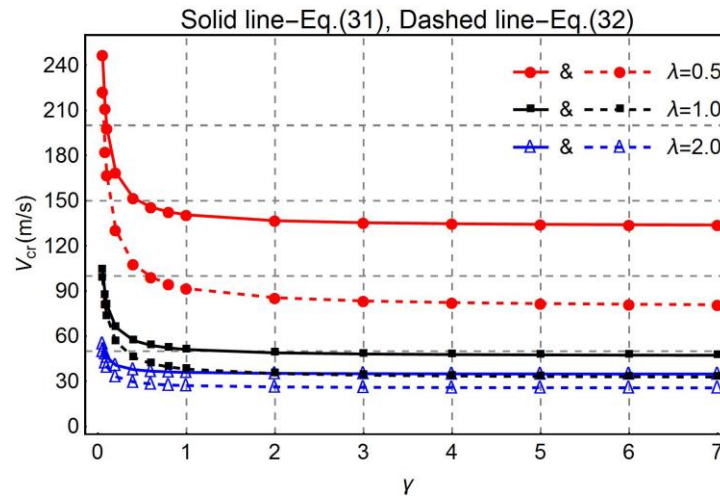
5.2 Along-wind span a

Let $m=n=1$, $\gamma=1$, $f=1$ m, $N_{0x}=2$ kN/m, and $\lambda=0.5$, 1, 2. Then the curves of along-wind span and critical wind velocity are calculated by Eqs. (31) and (32) and shown in Fig. 3.

From Fig. 3, at different λ, all the critical wind velocities that calculated by Eqs. (31) and (32) decrease gradually with the increasing of span a. They decrease sharply when $a < 30m$ and decrease gently when $a > 30$ m. This shows that the span size should not be taken too large in the design, thus to prevent it from being destroyed in the wind. In addition, the critical wind velocity values calculated by Eq. (31) are all greater than the corresponding results calculated by Eq. (32). Meanwhile, the differences between them decrease with the increasing of the span a and the span ratio λ.

5.3 Pretension N_{0x}

Let $m=n=1$, $\gamma=1$, $K=1$ m, $a=20$ m, and $\lambda=0.5$, 1, 2. Then the curves of pretension N_{0x} and critical wind velocity are calculated by Eqs. (31) and (32) and shown in Fig. 4.

From Fig. 4, we can see that all the critical wind velocities that calculated by Eqs. (31) and (32) increase gradually with increasing of pretension N_{0x}, and all of them present weak nonlinearity in general. This shows that we should apply a certain pretension to membrane structures and reinforce the structure in time after the relaxation of the membrane in engineering practices to grantee the safety of the structure. In addition, the critical wind velocities calculated by Eq. (31) are all greater than the corresponding results that calculated by Eq. (32); and the relative differences between them decrease with increasing of λ.

Fig. 4 Curves of pretension N_{0x} and critical wind velocity V_{cr}

Fig. 5 Curves of N_{0x}-to-N_{0y} ratio γ and critical wind velocity V_{cr}

5.4 N_{0x}-to-N_{0y} ratio γ

Let $m=n=1$, $K=1$ m, $a=20$ m, $N_{0x}=2$ kN/m and $\lambda = 0.5$, 1, 2. The curves of N_{0x}-to-N_{0y} ratio γ and critical wind velocity are calculated by Eqs. (31) and (32) and shown in Fig. 5.

Form Fig. 5, we can see that all the critical wind velocities that calculated by Eqs. (31) and (32) decrease with increasing of N_{0x}-to-N_{0y} ratio γ when N_{0x} keeps constant, and all of them present strong nonlinearity in general. The critical wind velocities decrease sharply when $\gamma < 1$, and

decrease gently when $\gamma > 1$. This shows that the critical wind velocity will decrease with decreasing of N_{0y} when N_{0x} keeps constant. In addition, the critical wind velocity values that calculated by Eq. (31) are all greater than the corresponding results that calculated by Eq. (32); and the relative differences between them increase with increasing of γ.

5.5 Amplitude f

Let $m=n=1$, $\gamma=1$, $a=20$ m, $N_{0x}=2$ kN/m and $\lambda = 0.5$, 1, 2. The curves of the amplitude f and critical wind velocity are calculated by Eqs. (31) and (32) and shown in Fig. 6.

Form Fig. 6, we can see that all the critical wind velocities that calculated by Eqs. (31) and (32) increase with increasing of amplitude f. When $f \to 0$, V_{cr} is equal to the results based on the small amplitude (linear) theory. In addition, the critical wind velocity values that calculated by Eq. (31) are all greater than the corresponding results that calculated by Eq. (32); and the relative differences between them increase with increasing of f.

5.6 Mode shapes in terms of orders m, n

Let $\gamma=1$, $a=20$ m, $f=1$ m, $N_{0x}=2$ kN/m and $\lambda = 0.25$, 0.5, 1, 2, 4. The critical wind velocities with different orders are shown in Table 1.

From Table 1, we can see that span ratio $\lambda < 1$ triggers higher-order instability mode along x direction ($m>n=1$); and the smaller λ is, the higher order (m) the instability will occur on. In opposite, span ratio $\lambda > 1$ triggers lower-order instability both in x and y directions ($m = n =1$). In addition, in Table 1, the critical wind velocity values that calculated by Eq. (31) are all greater than the corresponding results that calculated by Eq. (32); and the relative differences between them grow with increasing of orders.
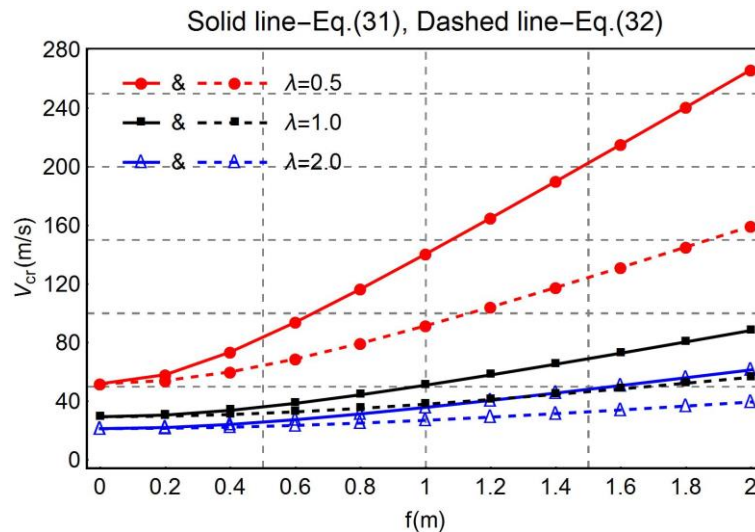

Fig. 6 Curves of amplitude K and critical wind velocity V_{cr}

Table 1 Critical wind velocity Vcr of different orders

Order	m=1,n=1	m=2,n=1	m=3,n=1	m=1,n=2	m=1,n=3	m=2,n=2	m=3,n=3
λ=0.25	595.024	351.806	**294.336**	3769.1	10060.6	1889.64	3504.18
	(355.28)	(210.72)	(**176.162**)	(2194.66)	(5830.47)	(1100.68)	(2031.19)
λ=0.5	139.76	**115.002**	154.072	703.017	1863.45	383.831	706.079
	(91.0687)	(**73.4078**)	(94.12)	(419.761)	(1092.21)	(229.901)	(414.654)
λ=1	**50.7397**	81.0667	138.356	152.009	371.835	119.715	214.071
	(**37.8223**)	(52.147)	(84.0435)	(99.0505)	(227.638)	(76.4159)	(129.94)
λ=2	**36.5098**	76.2041	132.916	52.5073	90.7771	82.5572	145.179
	(**27.5547**)	(48.559)	(80.4944)	(39.1398)	(62.9378)	(53.1058)	(88.5064)
λ=4	**33.961**	75.5349	133.344	36.9687	44.1043	77.1299	133.529
	(**25.2431**)	(47.9736)	(80.6845)	(27.901)	(33.4516)	(49.1489)	(80.9736)

Annotation:

(1) Values without brackets are calculated by Eq. (31); values in brackets are calculated by Eq. (32);

(2) The underlined and bold values represent critical instability modes triggered by the wind load.

6. Conclusions

The nonlinear aerodynamic stability of plane orthotropic membrane structure was studied by the analytical method. The critical velocity formula (31) was obtained considering the two characteristics of orthotropy and geometric nonlinearity. Comparing with formula (32), the effects of parameters were analyzed. The main conclusions are summarized as follows:

●   The span and span ratio λ of the plane membrane structure have a remarkable effect on the critical wind velocity. Generally, the critical wind velocity decrease with increasing of span, and the more different between the two span sizes (a and b) are, the greater the critical wind velocity is. Additionally, it has positive significance to arrange the membrane's warp and weft rationally according to the local wind regime to prevent instability of the plane membrane structure.

●   The pretension and amplitude will also affect the critical wind velocity. The critical wind velocity grows with the increase of pretension and amplitude. Meanwhile, the stress increment, which is acquired from the geometric nonlinearity, can improve the lateral stiffness and enhance the aerodynamic stability of structures.

●   Different mode shapes represented by the order number m and n exhibit different critical wind velocities. Generally, higher-order divergence instability occurs when the span ratio $\lambda < 1$; and lowest-order ($m=n=1$) divergence instability occurs when the span ratio $\lambda < 1$.

●   The critical wind velocities calculated by Eq. (31) are all greater than the corresponding results calculated by Eq. (32). This is because Eq. (31) is derived based on the stress function that fully satisfies the stress boundary conditions, but the stress function that result in Eq. (32) did not fully satisfy the stress boundary conditions. Therefore, Eq. (31) is more accurate.

In summary, the critical wind velocity formula (31) obtained in this paper provides a more accurate theoretical foundation for the aerodynamic stability of plane membrane structures. Meanwhile, we should comprehensively consider the effects of various factors on the design of membrane structures.

Acknowledgments

References

Attar, P.J. and Dowell, E.H. (2005), "A reduced order system ID approach to the modeling of nonlinear structural behavior in aeroelasticity", *J. Fluid Struct.*, **21**(5), 531-542.

Dowell, E.H. (1970), "Panel flutter: A review of the aeroelastic stability of panel and shells", *AIAA J.*, **8**(3), 385-399.

Forsching, H.W. (1980), "Principles of Aeroelasticity", *Shanghai Science & Technology Press*, Shanghai. (in Chinese)

Glück, M., Breuer, M., Durst, F., Halfmann, A. and Rank, E. (2001). "Computation of fluid-structure interaction on lightweight structures", *J. Wind Eng. Ind. Aerod.*, **89**(14), 1351-1368.

Ivovich, V.A. and Pokrovskii, L.N. (1991), "Dynamic analysis of suspended roof systems", A. A. Balkema, Rotterdam.

Kawakita, S., Bienkiewicz, B. and Cermak, J.E. (1992), "Aerolelastic model study of suspended cable roof", *J. Wind Eng. Ind. Aerod.*, **42** (1), 1459-1470.

Kornecki, A., Dowell E.H. and O'Brien, J. (1976), "On the aeroelastic instability of two-dimensional panels in uniform incompressible flow", *J. Sound Vib.*, **47**(2), 163-178.

Liu, C.J., Zheng, Z.L., Jun, L., Guo, J.J., and Wu, K. (2013), "Dynamic analysis for nonlinear vibration of prestressed orthotropic membrane structure with viscous damping", *Int. J. Struct. Stab. Dy.*, **13**(2), Article ID 1350018, 32 pages.

Liu, C.J., Zheng, Z.L., Yang, X.Y., and Zhao, H. (2014), "Nonlinear damped vibration of pre-stressed orthotropic membrane structure under impact loading", *Int. J. Struct. Stab. Dy.*, **14**(1), Article ID 1350055, 24 pages.

Lu, D., Lou, W.J. and Yang, Y. (2013), "Numerical calculation on wind-induced damping of membrane structure based on fluid-structure interaction", *J. Vib. Shock*, **6**, 011.

Luo Y.C. (2006), "The accident analysis of membrane structures and several aspects to structural design", *Spec. Struct.*, **23**(1), 26-29.

Michalski, A., Kermel, P.D., Haug, E., Löhner, R., Wüchner, R. and Bletzinger, K U. (2011), "Validation of the computational fluid–structure interaction simulation at real-scale tests of a flexible 29m umbrella in natural wind flow", *J. Wind Eng. Ind. Aerod.*, **99**(4), 400-413.

Minarni, H., Okuda, Y. and Kawamura, S. (1993), "Experimental studies on the flutter behavior of membranes in a wind tunnel", *Space Struct.*, **4**, 935-945.

Miyake, A., Yoshimura, T. and Makino, M. (1992), "Aerodynamic instability of suspended roof modals", *J. Wind Eng. Ind. Aerod.*, **42**(1), 1471-1482.

Scott, R.C., Bartels, R.E. and Kandil, O.A. (2007), "An aeroelastic analysis of a thin flexible membrane", *Proceedings of the 48th AIAA/ASME/ASCE/AHS/ASC Structures, Structural Dynamics and Materials*

Conference, Honolulu, Hawaii, April.

Shin, C.J., Kim, W. and Chung, J.T. (2004), "Free in-plane vibration of an axially moving membrane", *J. Sound Vib.*, **272**(1-2), 137-154.

Stanford, B. and Sytsma, M. (2007), "Static aeroelastic model validation of membrane micro air vehicle wings", *AIAA J.*, **45**(12), 2828-2837.

Stanford, B. and Ifju, P. (2008), "Fixed membrane wings for micro air vehicles: Experimental characterization, numerical modeling, and tailoring", *Prog. Aerosp. Sci.*, **44**(4), 258-294.

Sun, B.N., Mao G.D. and Lou, W.J. (2003), "Wind induced coupling dynamic response of closed membrane structures", *Proceedings of the 11th International Conference on Wind Engineering*, Sanya, Hainan, Dec.

Sun, F.J., and Gu, M. (2014), "A numerical solution to fluid-structure interaction of membrane structures under wind action", *Wind Struct.*, **19**(1), 35-58.

Sygulski, R. (1994), "Dynamic analysis of open membrane structures interaction with air", *Int. J. Numer. Meth. Eng.*, **37**(11), 1807-1823.

Sygulski, R. (1997), "Numerical analysis of membrane stability in air flow", *J. Sound Vib.*, **201**(3), 281-292.

Sygulski, R. (1996). "Dynamic stability of pneumatic structures in wind: theory and experiment", *J. Fluid. Struct.*, **10**(8), 945-963.

Uematsu, Y. and Uchiyama, K. (1986), "Aeroelastic behavior of an H.P. shaped suspended roof", *Proceedings of the IASS Symposium on Membrane Structures and Space Frame*, Osaka, May.

Wu, Y., Chen, Z.Q., and Sun, X.Y. (2015), "Research on the wind-induced aero-elastic response of closed-type saddle-shaped tensioned membrane models", *J. Zhejiang Univ. Sci. A*, **16**(8), 656-668.

Wu, Y., Sun, X. and Shen, S. (2008), "Computation of wind-structure interaction on tension structures", *J. Wind Eng. Ind. Aerod.*, **96**(10), 2019-2032.

Xu, Y.P., Zheng, Z.L., Liu, C.J., Song, W.J. and Long, J. (2011), "Aerodynamic stability analysis of geometrically nonlinear orthotropic membrane structure with hyperbolic paraboloid", *J. Eng. Mech. - ASCE*, **137**(11), 759-768.

Yang, Q.S. and Liu, R.X. (2005), "On aerodynamic stability of membrane structures", *Int. J. Space Struct.*, **20**(3), 181-188.

Zhou, Y., Li, Y., Shen, Z., Wang, L. and Tamura, Y. (2014), "Numerical analysis of added mass for open flat membrane vibrating in still air using the boundary element method", *J. Wind Eng. Ind. Aerod.*, **131**, 100-111.

Zheng, Z.L., Xu, Y.P., Liu, C.J. He, X.T. and Song, W.J. (2011), "Nonlinear aerodynamic stability analysis of orthotropic membrane structures with large amplitude", *Struct. Eng. Mech.*, **37**(4), 401-413.

CC